Chenggang Li ✉
Wenyan Zhang
Jing Chen
Jingjing You

https://doi.org/10.21278/TOF.454003219
ISSN 1333-1124
eISSN 1849-1391

A COMPARATIVE STUDY ON TWO METHODS OF DECOUPLING A SIX-AXIS ACCELEROMETER WITHOUT AND WITH A GYROSCOPE

Summary

Methods of decoupling a 6-axis accelerometer are attracting more and more attention because of their great significance for the accuracy, efficiency and stability of acceleration calculation. This paper introduces the basic decoupling methods without and with a gyroscope first. The decoupling accuracies of numerical accelerations are compared based on the definition of the comprehensive error, and the efficiencies are compared based on the computational time. In order to compare the stability of the two methods, the influence of step size is given, and the comprehensive errors are compared. Possible error sources that affect the stability of the decoupling methods are listed and divided into three categories, and the influence of every error source is analysed and presented. In the simulation, the gyroscope-based method is verified to achieve better accuracy, efficiency and stability than in the case of the method without a gyroscope. The experimental results agree well with the theoretical analysis.

Key words: *6-axis accelerometer, decoupling methods, gyroscope, decoupling accuracy, stability*

1. Introduction

The 6-axis accelerometer plays an important role in measuring the omni-directional motion of an object, and has a wide application prospect in the fields of vibration measurement, dynamics control, aerospace test, human motion measurement, consumer equipment and other fields [1~3]. The configuration design, decoupling calculation, parameter calibration, experiments of the 6-axis accelerometer have attracted much attention of researchers [4~12], and the measurement accuracy of the sensor is one of the important performances of the actual sensor. However, there are few prototypes with perfect accuracy that have been used in practical applications as the structure of a 6-axis sensor is complex and a lot of errors are introduced from the decoupling method, signal processing, etc. In the decoupling processing, some differential methods are used to solve the angular velocity in order to obtain the final acceleration, which decreases the final accuracy of the sensor. Ref [4] estimated the angular velocity and angular acceleration in an unmanned aerial vehicle (UAV) by using *N* linear accelerometers, but the accuracy was not improved much compared with the case when angular-rate sensors are used directly. Ref [5] also built gyro-free inertial

navigation system models based on a conventional 6-accelerometer cube, and a hardware prototype was implemented. The computed motions from the accelerometers had small errors during the few seconds, and the errors were accumulated quickly over time. Ref [6] proposed a 6-DOF acceleration sensing method by decoupling the outputs from six coplanar single-axis accelerometers, and the 6-DOF acceleration could be sensed and measured accurately when the sensed angular velocity was low. Further, Ref [13] derived the dynamics of a 6-axis accelerometer using the Newton-Euler method, and an "auxiliary angular velocity" was proposed for simplifying the numerical calculation.

There are also many papers on the accuracy calibration of triaxial accelerometers with a gyroscope. In [14], Ref derived the calibration method for a triaxial accelerometer with a triaxial gyroscope, which was used to calibrate the accelerometer in a smartphone. Ref [15] also presented a design of a fuzzy rule base aiming at merging the measurements by a micro-accelerometer and three gyroscopes, and allowed compensation for the gyroscope's drift in a steady state and accelerometers' drift during rotation. Other methods for accelerometer calibration were also proposed by Ref [16, 17]. However, these papers focused only on some conventional triaxial accelerometers.

This paper focuses on the comparison of performance of two methods of decoupling the 9-SPS parallel type 6-axis accelerometer described by Ref [13] and [18], without and with a gyroscope. The gyroscope is assumed to be calibrated well and be accurate for a short period of time, and the 6-axis accelerometer's drift is not considered in this paper. In section 2, the 6-axis accelerometer is introduced. Its original decoupling method is denoted based on Newton-Euler equations presented in section 3. The novel decoupling method with a gyroscope is proposed in section 4. Section 5 gives a comparison of two decoupling methods in some aspects of accuracy, efficiency, and stability. The experiment and results are presented in section 6.

2. Configuration of a 6-axis accelerometer

The 6-axis accelerometer uses a parallel mechanism as the elastic body, and a piezoelectric ceramic as a sensitive component. The sensor shown in Fig. 1 is composed of a cubic block, piezoelectric ceramics, spherical joints, a housing, and other components.

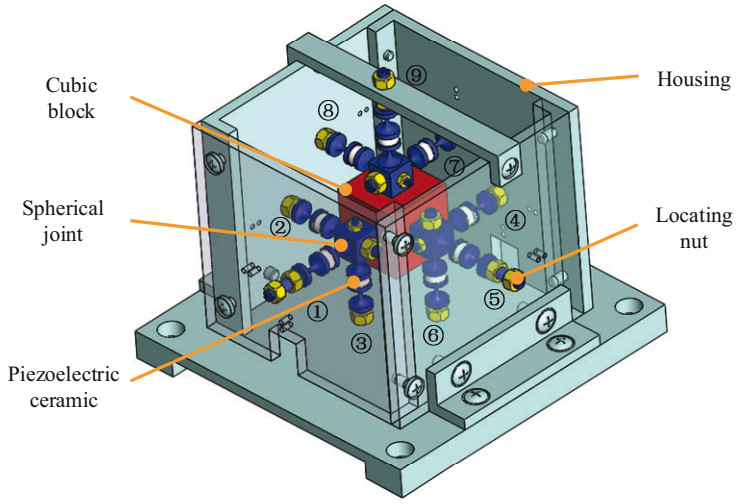

Fig. 1 3D model of a parallel type 6-axis accelerometer

In Fig.1, numerals ① to ⑨ correspond to 9-SPS (S represents the spherical joints and P the prismatic pairs) branch chain numbers. When the housing is rigidly attached to the carrier and subjected to acceleration of the carrier, since each branch can be regarded as a two-pole rod, each branch produces a corresponding axial force f_i. The axial forces are sensed by the piezoelectric ceramics and are input signals for the sensor system. Because of the high

stiffness of the piezoelectric ceramics, the relative motion between the cubic block and the housing is negligible. Therefore, the absolute linear acceleration and angular acceleration of the cubic block centre are the 6-axis absolute accelerations of the carrier.

3. Decoupling method based on Newton-Euler equations

A diagram of 9-SPS parallel type 6-axis accelerometer is shown in Fig. 2, in which b_i (i=1~3) represents the position coordinate of the spherical joint, P_i (i=1~9) the prismatic pair, and B_{ij} (i=1~3, j=1~3) the position coordinate of the outside spherical joint. Inertial frame $\{O\}$ is established at the centre of the cubic block, and the x/y/z axes are parallel to the branches ③, ② and ④ in Fig. 1, respectively. Block frame $\{M\}$, which coincides with frame $\{O\}$ initially, is fixed on the cubic block.

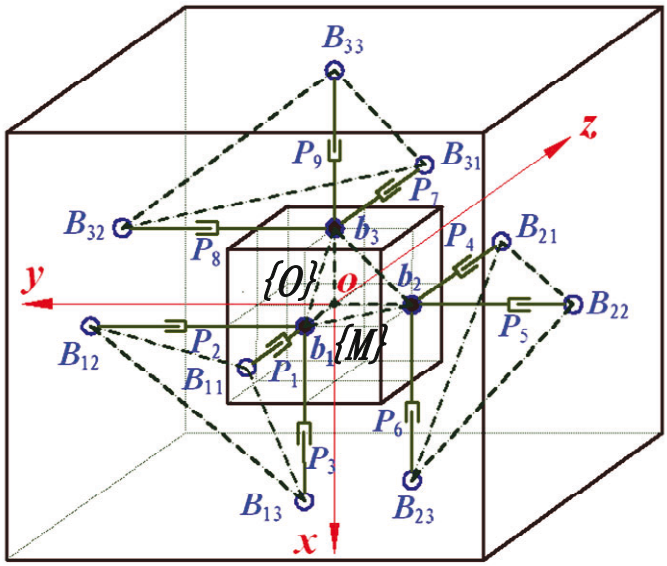

Fig. 2 Diagram of a parallel type 6-axis accelerator

Linear acceleration $\boldsymbol{a}^O$ and angular acceleration $\boldsymbol{\varepsilon}^O$ can be expressed as [19],

$$\begin{bmatrix} \boldsymbol{a}^O \\ 0 \end{bmatrix} = \frac{1}{m} \boldsymbol{A}_M^O \begin{bmatrix} -f_3 - f_6 + f_9 \\ -f_2 + f_5 - f_8 \\ f_1 - f_4 - f_7 \\ 0 \end{bmatrix} + \begin{bmatrix} g \\ 0 \\ 0 \\ 0 \end{bmatrix} \tag{1}$$

$$\begin{bmatrix} \boldsymbol{\varepsilon}^O \\ 0 \end{bmatrix} = \frac{3}{2mn} \boldsymbol{A}_M^O \begin{bmatrix} -f_2 + f_4 \\ f_3 - f_7 \\ -f_6 + f_8 \\ 0 \end{bmatrix} \tag{2}$$

where f_i denotes the axial force of the i^{th} branch (i=1~9), m the mass of the cubic block, n the half-length of the cubic block, and g the gravitational acceleration value. $\boldsymbol{A}_M^O$ is a 4×4 rotation matrix of frame $\{M\}$ with respect to frame $\{O\}$ and in the form of quaternions $\{\xi_0, \xi_1, \xi_2, \xi_3\}$ as follows:

$$\boldsymbol{A}_M^O = (\boldsymbol{\Phi}^-)^T \boldsymbol{\Phi}^+$$

with

$$\boldsymbol{\Phi}^{-}=\begin{bmatrix}\xi_0 & \xi_3 & -\xi_2 & \xi_1\\ -\xi_3 & \xi_0 & \xi_1 & \xi_2\\ \xi_2 & -\xi_1 & \xi_0 & \xi_3\\ -\xi_1 & -\xi_2 & -\xi_3 & \xi_0\end{bmatrix} \text{ and } \boldsymbol{\Phi}^{+}=\begin{bmatrix}\xi_0 & -\xi_3 & \xi_2 & \xi_0\\ \xi_3 & \xi_0 & -\xi_1 & \xi_1\\ -\xi_2 & \xi_1 & \xi_0 & \xi_2\\ -\xi_1 & -\xi_2 & -\xi_3 & \xi_0\end{bmatrix}.$$

Eqs. (1) and (2) are both nonlinear and tightly coupled because of $\boldsymbol{A}_M^O$, so they cannot be solved directly. Auxiliary angular velocity $\boldsymbol{\omega}^*$ is introduced so that absolute angular velocity $\boldsymbol{\omega}^O$ of the cubic block can be written as

$$\begin{bmatrix}\boldsymbol{\omega}^{\boldsymbol{O}}\\ \mathbf{0}\end{bmatrix}=\boldsymbol{A}_{\boldsymbol{M}}^{\boldsymbol{O}}\begin{bmatrix}\boldsymbol{\omega}^*\\ \mathbf{0}\end{bmatrix} \tag{3}$$

With the knowledge of quaternions, $\boldsymbol{\omega}^O$ can also be described as

$$\begin{bmatrix}\boldsymbol{\omega}^O\\ 0\end{bmatrix}=2\left(\boldsymbol{\Phi}^{-}\right)^T\left(\frac{\mathrm{d}}{\mathrm{d}t}\left[\xi_1,\xi_2,\xi_3,\xi_0\right]^T\right) \tag{4}$$

Take the first derivation on both sides of Eq. (3) simultaneously, and $\frac{\mathrm{d}}{\mathrm{d}t}\boldsymbol{A}_M^O=\begin{bmatrix}\boldsymbol{\omega}^O\\ 0\end{bmatrix}\times\boldsymbol{A}_M^O$ is known, then

$$\begin{bmatrix}\boldsymbol{\varepsilon}^O\\ 0\end{bmatrix}=\left(\frac{d}{dt}\boldsymbol{A}_M^O\right)\begin{bmatrix}\boldsymbol{\omega}^*\\ 0\end{bmatrix}+\boldsymbol{A}_M^O\frac{\mathrm{d}}{\mathrm{d}t}\begin{bmatrix}\boldsymbol{\omega}^*\\ 0\end{bmatrix}=\boldsymbol{A}_M^O\begin{bmatrix}\boldsymbol{\omega}^*\\ 0\end{bmatrix}\times\boldsymbol{A}_M^O\begin{bmatrix}\boldsymbol{\omega}^*\\ 0\end{bmatrix}+\boldsymbol{A}_M^O\frac{\mathrm{d}}{\mathrm{d}t}\begin{bmatrix}\boldsymbol{\omega}^*\\ 0\end{bmatrix}=\boldsymbol{A}_M^O\frac{\mathrm{d}}{\mathrm{d}t}\begin{bmatrix}\boldsymbol{\omega}^*\\ 0\end{bmatrix} \tag{5}$$

Combining Eqs. (2) with (5) yields

$$\frac{\mathrm{d}}{\mathrm{d}t}\begin{bmatrix}\boldsymbol{\omega}^*\\ 0\end{bmatrix}=\frac{3}{2mn}\begin{bmatrix}-f_2+f_4\\ f_3-f_7\\ -f_6+f_8\\ 0\end{bmatrix} \tag{6}$$

Combining Eqs. (3) with (4) yields

$$\frac{\mathrm{d}}{\mathrm{d}t}\left[\xi_1,\xi_2,\xi_3,\xi_0\right]^T=\frac{1}{2}\boldsymbol{\Phi}^{+}\begin{bmatrix}\boldsymbol{\omega}^*\\ 0\end{bmatrix} \tag{7}$$

Suppose that the motion parameters of the 6-axis accelerometer at the initial state are:

$$\begin{cases}\boldsymbol{\omega}^*{}_{(0)}=\left[0,0,0\right]^T\\ \left[\xi_1,\xi_2,\xi_3,\xi_0\right]_{(0)}=\left[0,0,0,1\right]\end{cases} \tag{8}$$

By using the improved Euler method and Eqs. (6) ~ (8), the auxiliary angular velocity and acceleration at *N* instant could be derived based on the values at *N*-1 instant as follows:

$$\boldsymbol{\omega}^*_{(N)} = \boldsymbol{\omega}^*_{(N-1)} + \frac{\boldsymbol{r}}{2}\left(\frac{\mathrm{d}}{\mathrm{d}t}\boldsymbol{\omega}^*_{(N-1)} + \frac{\mathrm{d}}{\mathrm{d}t}\boldsymbol{\omega}^*_{(N)}\right) \tag{9}$$

$$\begin{bmatrix} \xi_{1(N)} \\ \xi_{2(N)} \\ \xi_{3(N)} \\ \xi_{0(N)} \end{bmatrix} = \boldsymbol{\Phi}^+_{(N-1)} \begin{bmatrix} \frac{r}{4}\left(\boldsymbol{\omega}^*_{(N-1)} + \boldsymbol{\omega}^*_{(N)}\right) + \frac{r^2}{8}\boldsymbol{\omega}^*_{(N-1)} \times \boldsymbol{\omega}^*_{(N)} \\ 1 - \frac{r^2}{8}\boldsymbol{\omega}^*_{(N-1)} \cdot \boldsymbol{\omega}^*_{(N)} \end{bmatrix} \tag{10}$$

where r is the step size.

Substituting Eq. (9) into Eq. (10), a solution for the quaternions and the rotation matrix $\boldsymbol{A}_M^O$ could be obtained. Then substituting $\boldsymbol{A}_M^O$ and f_i into Eqs. (1) and (2), linear acceleration $\boldsymbol{a}^O$ and angular acceleration $\boldsymbol{\varepsilon}^O$ can be obtained.

4. Decoupling method with a gyroscope

Although the Newton-Euler method has advantages of high efficiency and adaptability, round-off error and truncation error are inevitably introduced. The error accumulation effect will emerge and increase with an increase in the calculation time [19].

According to section 2, the physical nature of auxiliary angular velocity $\boldsymbol{\omega}^*$ is the velocity projection of the cubic block velocity in inertial frame $\{O\}$. Introduce a gyroscope in the measurement system, then fix the gyroscope and the 6-axis accelerometer to the carrier. The measurement value from the gyroscope $\boldsymbol{\omega}^t$ is just the same physical quantity as $\boldsymbol{\omega}^*$ when the relative motion between the block and the housing is neglected. Therefore, the quaternions can be solved by replacing $\boldsymbol{\omega}^*$ in Eqs. (7)-(10) with $\boldsymbol{\omega}^t$, and the 6-axis acceleration components can be obtained from Eqs. (1) and (2). Because of the introduction of the gyroscope, Eqs. (6) and (9) for solving the auxiliary angular velocity are not necessary, which not only reduces the computational complexity, but also partially avoids the iterative calculation.

In order to be simple and intuitive, the original method of decoupling the 6-axis accelerometer is denoted as the Non-gyro method, and the method with a gyroscope is denoted as the Gyro method. A comparative chart of the two solutions of the decoupling methods is shown in Fig. 3.

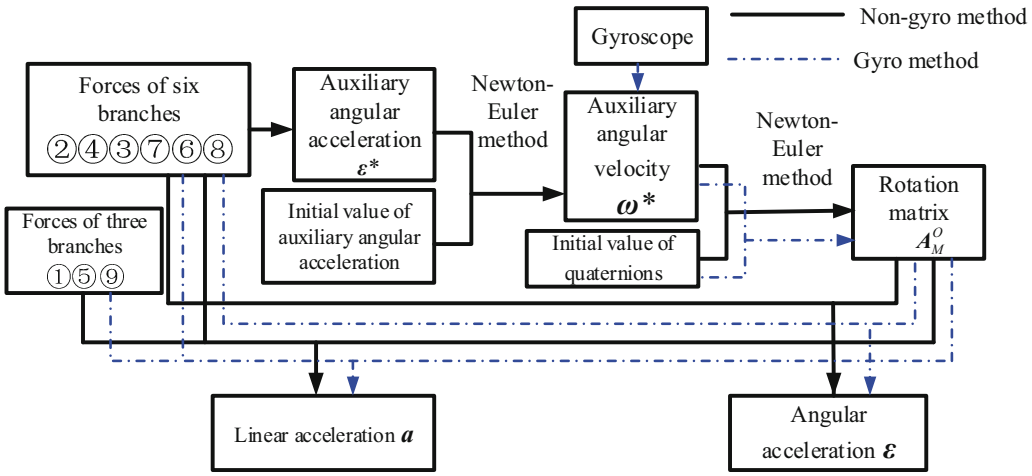

Fig. 3 Comparative chart of two decoupling methods

5. Comparison of two decoupling methods

5.1 Comparative analysis of accuracy and computational efficiency

The accuracy and computational efficiency of numerical acceleration are very important indicators for the decoupling method. The comprehensive error is specified as the mean value of three calculated linear acceleration errors and three calculated angular acceleration errors, and it is employed to evaluate the calculation accuracy. The computational time is used to evaluate the computational efficiency as by Ref [19]. Random disturbances whose elements are normally distributed with mean 0 and variance 1 are introduced to the output of the sensing elements, the initial values of quaternions, the auxiliary angular velocity, the block mass, and the half-length of the block at the same time. The amplitudes of these disturbances are set to be 0.009 N, 0.009, 0.09 rad/s, 0.009 Kg and 0.9 mm, respectively. Numerical simulations are carried out in 5 seconds, and data are filtered by the mean value of six samples.

The comprehensive errors and computational time consumptions using two decoupling methods are plotted in Fig. 4. The error bars are shown in Fig. 4(a).

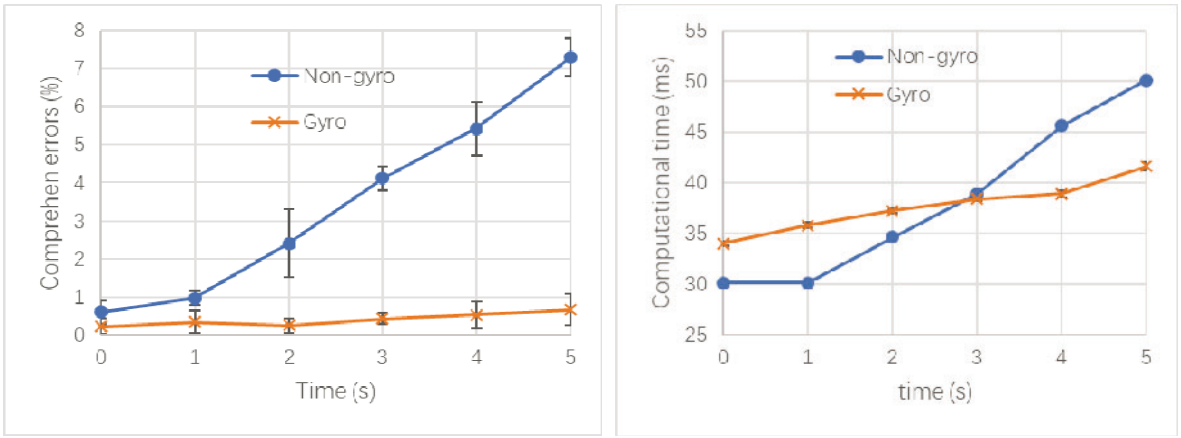

(a) Comprehensive errors (%) (b) Computational time (ms)

Fig. 4 Comprehensive errors of and computational time for two decoupling methods

In Fig. 4, it is clear that:

(1) In terms of comprehensive errors and computational time, the Gyro method has more advantages than the Non-gyro method. The comprehensive errors of the Gyro method are ten times bigger than that of the Non-gyro method, and the accuracy advantage of the Gyro method becomes more and more obvious as time goes by.

(2) Both methods can meet the real-time decoupling requirement. When the simulation time is short, the total computational times of the two methods are close, although the efficiency of the Gyro method is higher than that of the Non-gyro method over time.

5.2 Comparative analysis of stability

5.2.1 Influence of step size on stability

One concern of the numerical stability is the growth in round-off errors. Since the iterative numerical method is adopted in the two methods in this paper, the round-off errors are closely related to the step size. Therefore, it is necessary to study the influence of different steps on the two decoupling methods.

Different step sizes in the simulation are specified and the two decoupling methods are used to calculate the comprehensive errors. The simulation step sizes vary from 0.001 s to 0.009 s, and the comparison is shown in Fig. 5.

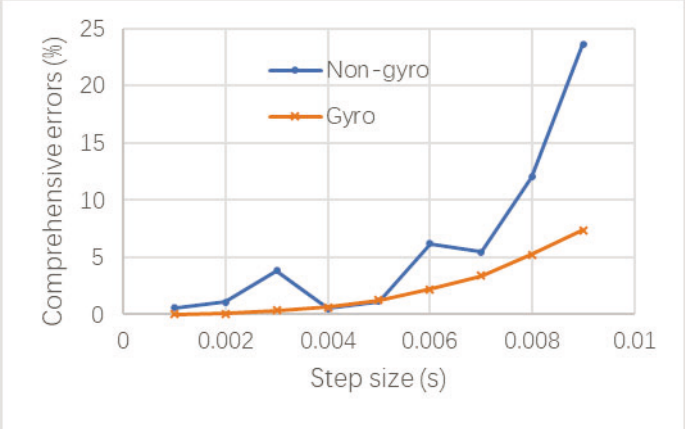

Fig. 5 Comparison of comprehensive errors of two methods with respect to different step sizes

It can be observed that:

(1) The comprehensive errors of the two decoupling methods increase as the step size increases, which reflects the sensitivity of the two decoupling methods to the step size.

(2) When the step size is not more than 0.005 s, the comprehensive errors of the two methods are close. With an increase in the step size, the comprehensive errors of the Non-gyro method obviously increase, and that of the Gyro method are relatively small.

(3) The comprehensive error trend of the Non-gyro method is fluctuating for different step sizes, and that of the Gyro method is quite steady. Hence, the Non-gyro method is more sensitive to the step size than the Gyro method.

5.2.2 Influence of disturbance on stability

(1) Error sources

In order to comprehensively compare and analyse the differences between the two decoupling methods, the error sources are listed and roughly divided into the following categories:

1) The output error of the sensing element, that is, the force error of each branch of the 6-axis accelerometer. Specify $\Delta f_{i(N)}$ to represent the error for the i^{th} branch at instant N.

2) The initial value error of the auxiliary angular velocity and that of the quaternions. Specify $\Delta\omega_0$ to represent the initial error of the auxiliary angular velocity and $\Delta\eta_0$ for that of the quaternions.

3) The parameter errors, mainly including the mass error and the half-length error of the cubic block. Specify Δm and Δn to represent them, respectively.

It should be noted that the gyroscope is introduced and regarded as a precise component, thus the output error of the gyroscope itself is neglected. The following flowcharts in Fig. 6 show the relationship among the error sources in the two methods of decoupling the 6-axis accelerometer.

Influences of the Non-gyro method and the Gyro method are analysed for three kinds of error sources.

(2) Comparative analysis of the output error of the sensing elements

The simulation is carried out in 10 seconds, the output error amplitudes are set from 0 to 0.009N, and the random disturbances whose elements are normally distributed with mean 0 and variance 1 are added to each specified output error amplitude. The disturbance effects of the two decoupling methods and error bars are plotted in Fig. 7, which shows the following:

1) The comprehensive errors of the decoupling methods increase with an increase in the sensor output disturbance, which reflects the sensitivity of the two decoupling methods to the sensor output disturbance.

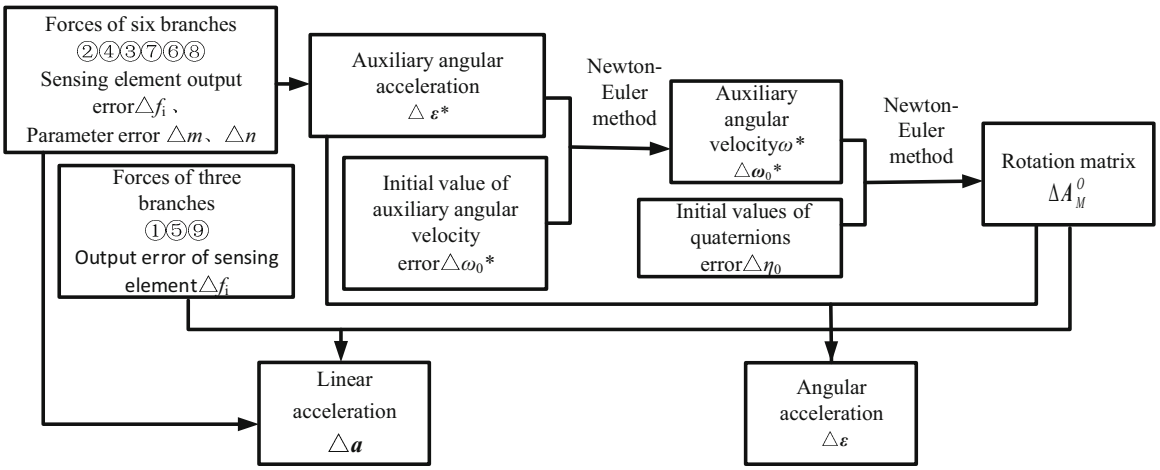

(a) Flowchart of the relationship among error sources without a gyroscope

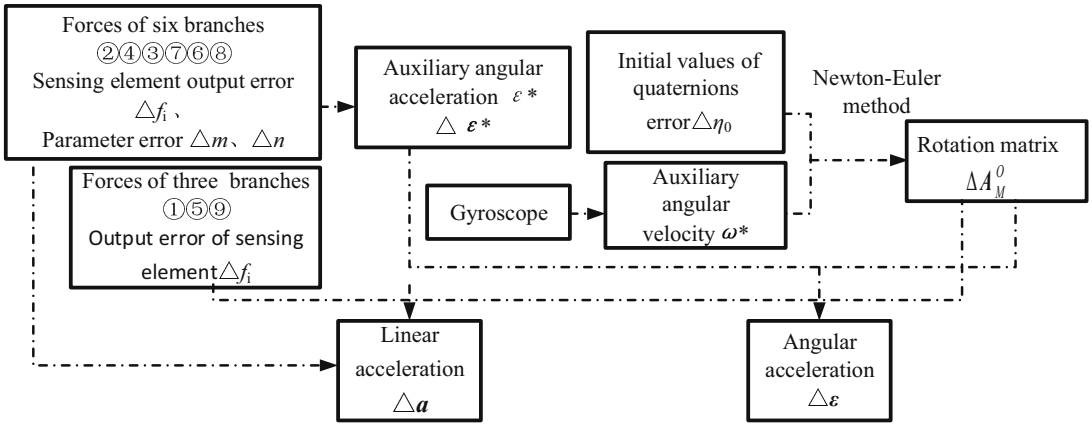

(b) Flowchart of the relationship among error sources with a gyroscope

Fig. 6 Flowcharts of error sources in two decoupling methods

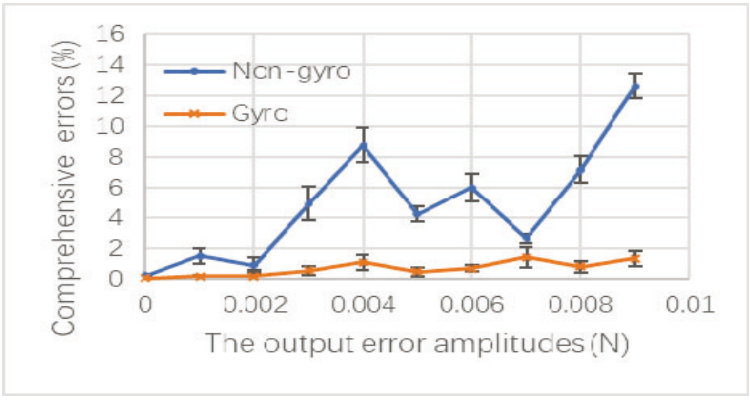

Fig. 7 Comparison of comprehensive errors of two methods with respect to output disturbances

2) The comprehensive error trend line of the Non-gyro method is steeper with respect to the sensor output disturbance, while that of the Gyro method is relatively flat. The reason could be that the output disturbance only affects the Gyro method in the dynamic solution, while it affects the Non-gyro method in the case of the auxiliary angular velocity, the rotation matrix and the dynamic solution.

(3) Comparative analysis of disturbance from auxiliary angular velocity and quaternions

The simulation is carried out in 10 seconds, and the disturbance amplitudes are set from 0 to 0.09 degree/s on the auxiliary angular velocity and from 0 to 0.009 on the initial values of quaternions. The random noises whose elements are normally distributed with mean 0 and variance 1 are added to each specified disturbance amplitude. The influences of the two decoupling methods with both the auxiliary angular velocity and the quaternions are shown in Fig. 8. The error bars are also shown.

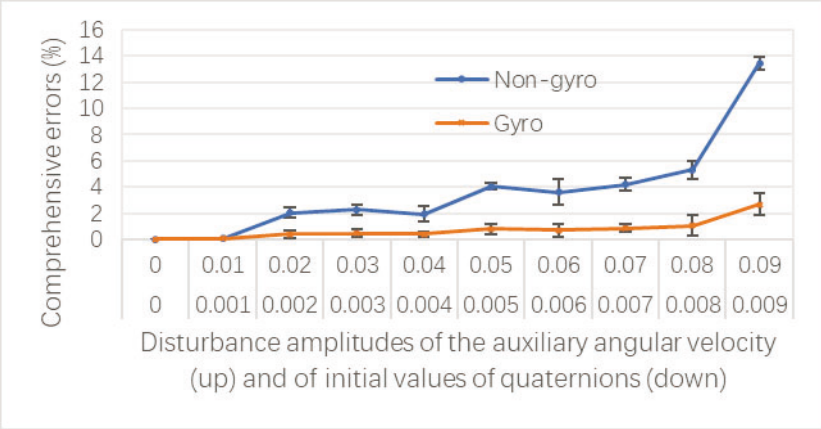

Fig. 8 Comparison of comprehensive errors of two decoupling methods with respect to disturbance from auxiliary angular velocity and quaternions

Fig. 8 shows that the comprehensive errors of the two decoupling methods tend to increase with both the increases in the disturbance amplitudes of the auxiliary angular velocity and in the initial values of quaternions. The error of the Gyro method is much smaller especially with higher abscissa values, which brings a greater advantage over Non-gyro.

The reasons could be that the auxiliary angular velocity in the Non-gyro method is calculated depending on the initial values of the auxiliary angular velocity, and the influence of the accumulated error caused by the double iterative numerical calculation is greater than that of the Gyro method.

(4) Comparison and analysis of parameter disturbance

The simulation is carried out in 10 seconds, and the parameter disturbance amplitudes are set from 0 to 0.009 Kg on the mass, and from 0 to 0.9 mm on the half-length of the cubic block. The random noises whose elements are normally distributed with mean 0 and variance 1 are added to each specified parameter disturbance amplitude. The influences of the two decoupling methods are given, and the error bars are also shown in Fig. 9.

In Fig. 9, it is clear that the comprehensive errors of the Non-gyro method and of the Gyro method increase with an increase in their disturbance amplitudes, and the comprehensive errors of the Non-gyro method are always slightly bigger than those of the Gyro method. This is because the mass parameter disturbances are introduced in the Non-gyro method and the Gyro method during the dynamic solution, and the half-length parameter disturbance is taken in the Non-gyro method during the process of solving the auxiliary angular velocity. Therefore, the Gyro method is superior to the Non-gyro method from the point of view of the accuracy with respect to the parameter disturbance.

According to the above analysis, it can be seen that the Gyro method is superior to the Non-gyro method in terms of accuracy, efficiency or numerical stability.

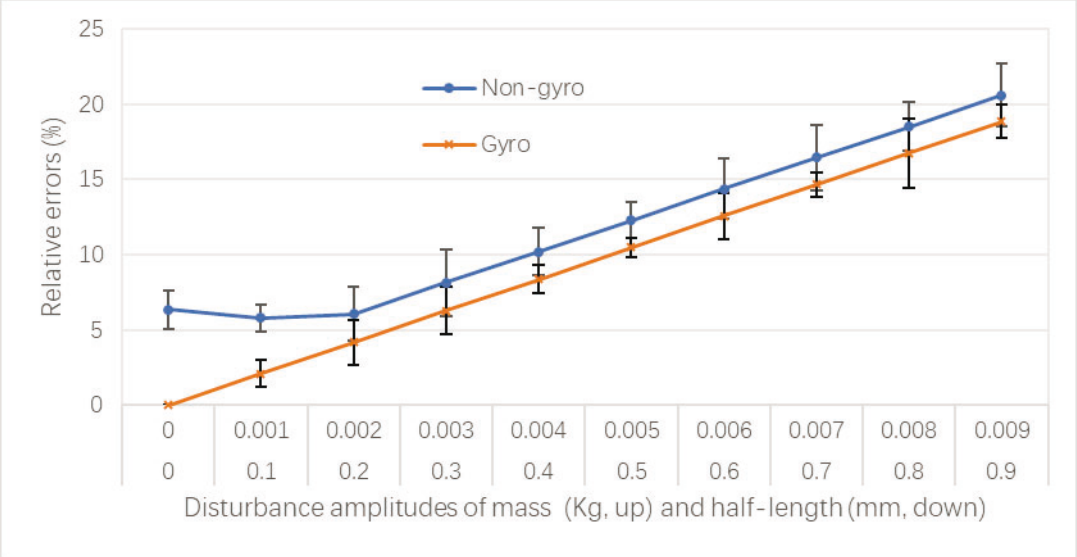

Fig. 9 Comparison of comprehensive errors of two decoupling methods with respect to parameter disturbances

6. Experiment and results

The experimental device shown in Fig. 10 consists of a motion platform, a 6-axis accelerometer prototype, a CRS03-04S gyroscope, a GINS100 MEMS Inertial Navigation System (INS) used as a backup, DC power supply, an Industrial Personal Computer (IPC) and a multi-channel charge amplifier. Data are collected at 500Hz in LABVIEW. The origin of the motion frame is fixed at the centre of the gyroscope to the motion platform, the x axis points downwards, the z axis inwards, and the y axis leftwards, the same as the *y* axis of the 6-axis accelerometer. The 6-axis accelerometer has the same angular velocity and acceleration as the gyroscope based on the gear and the gear rack mechanism. The INS will be fixed to the location of the gyroscope and the gyroscope is moved when the INS is used to measure angular velocity or angular acceleration.

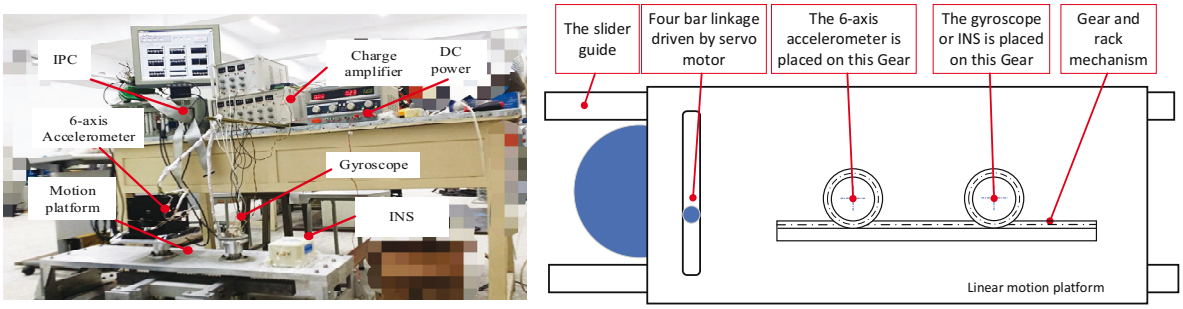

(a) Experimental setup (b) Diagram of the motion platform

Fig. 10 Experimental setup and diagram of 6-axis accelerometer

Because the linear acceleration errors are smaller than the angular acceleration errors in three direction as shown in Fig. 4(a), the angular accelerations only are tested in this section. The experiments are implemented in three tests to measure three angular accelerations in three directions. First, the 6-axis accelerometer is fixed in the position as shown in Fig. 10 and its frame matches with the frame of the motion platform. Second, the 6-axis accelerometer is rotated 90 degrees along its z-axis and fixed. Third, the 6-axis accelerometer is rotated -90 degrees along its y-axis and fixed.

In the experiment, the angular acceleration of the motion platform is specified as $5.64\cos(3.57\,t-\pi/2)$. The 6-axis accelerometer and the gyroscope move synchronously and

cyclically. Data are collected into a 16bit data acquisition card and filtered by the mean value of six samples. The decoupling calculations of the Non-gyro method and the Gyro method are carried out and compared with the angular acceleration output of the INS. The angular acceleration output error of the INS is ignored because the angular velocity accuracy of the INS is up to 0.008 degree/s, and the improved Euler method and the mean value filter are used. Fig. 11 (a)-(c) show the angular accelerations of the two decoupling methods and the measured angular accelerations. The absolute errors of the two decoupled methods are also plotted, as shown in the figures.

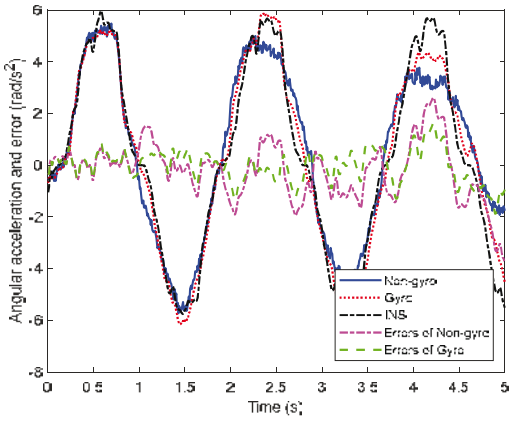

(a) In *x*-direction

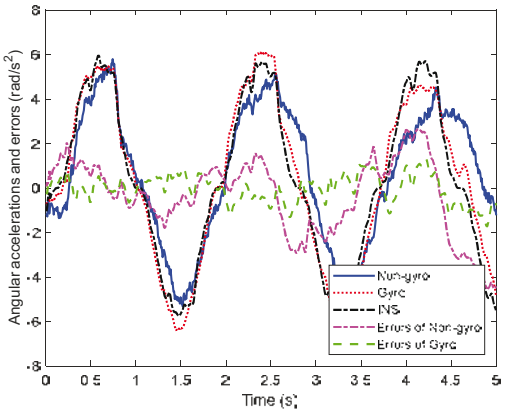

(b) In *y*-direction

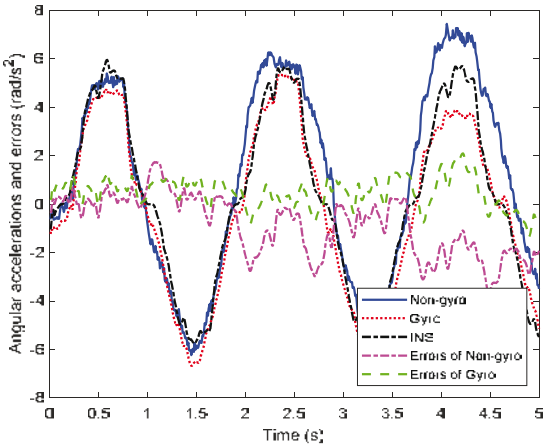

(c) In *z*-direction

Fig. 11 Comparison of three direction accelerations and errors

The accelerations in Fig. 11 show that the results of the two decoupling methods are consistent with the output of the INS in five seconds, which verifies the correctness of the two decoupling methods. Fig. 11 shows also that the errors of the two decoupling methods relative to the output of the INS increase over time which is in agreement with the error accumulation effect of the iterative method. At the same time, the error increasing trends of the Non-gyro method are obviously stronger than those of the Gyro method. The maximum errors of the Non-gyro method and the Gyro method are about 50% and 20% (relative to the angular acceleration amplitude of the motion platform) in five seconds, and the mean errors are about 17% and 8%, respectively. The advantage of the Gyro method referring to the decoupling accuracy is verified. The possible reasons for the difference between Fig. 11 and Fig. 4(a) are that the experimental errors are introduced from the errors of the INS, the gyroscope or the motion platform.

7. Conclusion

Two decoupling methods for the 6-axis accelerometer are proposed, one without and the other with a gyroscope. The simulations and experiments show that the 6-axis accelerometer has better performance with the aid of a gyroscope.

(1) By introducing "auxiliary angular velocity", the second-order nonlinear dynamic equations of the parallel type 6-axis accelerometer are converted to the first-order linear differential equations, and the auxiliary angular velocities and quaternions are solved by using the Newton-Euler method in turn.

(2) An external gyroscope is introduced to the measurement system. The initial value of the "auxiliary angular velocity" and the calculated values at each time interval in the original decoupling method are replaced by the output of the gyroscope, which reduces the number of iterations from two to one.

(3) The two decoupling methods are compared and analysed from the point of view of accuracy and efficiency. The results show that the accuracy of the Gyro method is higher than that of the Non-gyro method, which becomes more and more obvious as the time passes. The efficiencies of the two methods are close in the short period of time, and the efficiency of the Gyro method is higher than that of the Non-gyro method in the longer period of time.

(4) The two decoupling methods are compared and analysed from the point of view of stability. The results show that the Non-gyro method is more sensitive to the influence of the step size than the Gyro method, and the Non-gyro method is more sensitive to the effect of three types of error sources than the Gyro method.

(5) The experimental study is carried out with a motion platform. The results show that the two decoupling methods are correct, and that the Gyro method has a higher decoupling accuracy and better error convergence than the Non-gyro method in terms of decoupling accuracy.

Acknowledgments

This study was supported partly by the Aeronautical Science Foundation of China (Grant No. 201916052001) and the National Natural Science Foundation of China (Grand No. 51175263).

REFERENCES

[1] Staufer, P.; Gattringer, H. State estimation on flexible robots using accelerometers and angular rate sensors. *Mechatronics* **2012**, 22(8), 1043-1049. https://doi.org/10.1016/j.mechatronics.2012.08.009

[2] Li, T. S.; Chen, C.; Su, Y. Optical image stabilizing system using fuzzy sliding-mode controller for digital cameras. *IEEE Transactions on Consumer Electronics* **2012**, 58(2), 237-245. https://doi.org/10.1109/TCE.2012.6227418

[3] Akamatsu, T.; Dong, F.; Hirota, K. 3D measurement of a moving object using 3D accelerometer attached to moving camera, *2013 IEEE 8th International Symposium on Intelligent Signal Processing*, 2013, 71-76. https://doi.org/10.1109/WISP.2013.6657485

[4] Cardou, P.; Angeles, J. A Comparative Study of All-Accelerometer Strapdowns for UAV INS. *Symposium SET-092/RSY18/MSE on Advanced Sensor Payloads for UAV,* **2005**.

[5] Akeila, E.; Salcic, Z.; Swain, A. Implementation, calibration and testing of GFINS models based on six-accelerometer cube, *TENCON 2008 IEEE Region 10 Conference*, **2008**, 1-6. https://doi.org/10.1109/TENCON.2008.4766567

[6] Wang, D. H.; Yuan, G. A Six-Degree-of-Freedom Acceleration Sensing Method Based on Six Coplanar Single-Axis Accelerometers. *IEEE Transactions on Instrumentation and Measurement* **2011**, 60(4), 1433-1442. https://doi.org/10.1109/TIM.2010.2083331

[7] Chapsky, V.; Portman, V. T.; Sandler, B.-Z. Single-mass 6-DOF isotropic accelerometer with segmented PSD sensors. *Sensors and Actuators A: Physical* **2007**, 135(2), 558-569. https://doi.org/10.1016/j.sna.2006.10.024

[8] Cui, F.; Liu, W.; Chen, W.; Zhang, W.; Wu, X. Design, fabrication and levitation experiments of a micromachined electrostatically suspended six-axis accelerometer. *Sensors* **2011**, 11(12), 11206-11234. https://doi.org/10.3390/s111211206

[9] Amarasinghe, R.; Dao, D. V.; Toriyama, T.; Sugiyama, S. Development of miniaturized 6-axis accelerometer utilizing piezoresistive sensing elements. *Sensors and Actuators A: Physical* **2007**, 134(2), 310-320. https://doi.org/10.1016/j.sna.2006.05.044

[10] Chunzhan, Y.; Xinyi, Z.; Qingxuan, J.; Jianping, L. Structural research on a six-axis accelerometer for picking robot wrist. *International Agricultural Engineering Journal* **2011**, 20(2), 36-41.

[11] Yu, C. Z.; Zhang, X. Y.; Han, J. H.; Tian, L. C. Study on Static Characteristics of an Integrated Six-Axis Accelerometer Based on Parallel Mechanism. *Advanced Materials Research* **2010**, 129-131, 224-229. https://doi.org/10.4028/www.scientific.net/AMR.129-131.224

[12] Jianguo, L. I.; Cui, H.; Yang, T., Quaternion constrained filter algorithm for spacecraft attitude determination. *Journal of Harbin Institute of Technology* **2013**, 45(1), 35-40.

[13] Yuhui, X.; Chenggang, L.; Jingjing, Y. Influences Analysis of Configurations on the Performance of Parallel Type Six-Axis Accelerometers. *Transactions of FAMENA* **2013**, 2(37), 67-86.

[14] Olsson, F.; Kok, M.; Halvorsen, K.; Schön, T. B. Accelerometer calibration using sensor fusion with a gyroscope, *2016 IEEE Statistical Signal Processing Workshop (SSP)*, **2016**, 1-5. https://doi.org/10.1109/SSP.2016.7551836

[15] Koprinkova-Hristova, P.; Alexiev, K. Fuzzy merging of MEMS accelerometers and gyroscopes measurements, *2016 International Symposium on INnovations in Intelligent SysTems and Applications (INISTA),* **2016***,* 1-6. https://doi.org/10.1109/INISTA.2016.7571829

[16] Al-Rawashdeh, Y. M.; Elshafei, M.; El-Ferik, S. Passive attitude estimation using gyroscopes and all-accelerometer IMU, *2016 7th International Conference on Mechanical and Aerospace Engineering (ICMAE),* **2016***,* 368-376. https://doi.org/10.1109/ICMAE.2016.7549568

[17] Roan, P.; Deshpande, N.; Wang, Y.; Pitzer, B. Manipulator state estimation with low cost accelerometers and gyroscopes, *2012 IEEE/RSJ International Conference on Intelligent Robots and Systems,* **2012***,* 4822-4827. https://doi.org/10.1109/IROS.2012.6385893

[18] Li, C.; Wang, Y.; Chen, J.; You, J.; Rajnathsing, H. Fault Diagnosis in a Gyroscope-Based Six-Axis Accelerometer. *Transactions of FAMENA* **2018**, 42(3), 103-114. https://doi.org/10.21278/TOF.42307

[19] You, J.; Chenggang, L. I.; Hongtao, W. U. Research on Hamiltonian Dynamics of Parallel Type Six-axis Accelerometer. *Journal of Mechanical Engineering* **2012**, 48(15), 9-17. https://doi.org/10.3901/JME.2012.15.009

Submitted: 24.4.2019
Accepted: 22.10.2021

Associate Prof. Chenggang Li*
Jing Chen
College of Mechanical and Electrical Engineering
Nanjing University of Aeronautics and Astronautics
29 Yudao str., Nanjing 210016, China
Wenyan Zhang
Jingjing You
College of Mechanical and Electronic Engineering
Nanjing Forestry University
159 Longpan road, Nanjing 210037, China
*Corresponding author:
lichenggang@nuaa.edu.cn